Proceedings of the 21st ICSMGE, Vienna, Austria, 14 – 19 June 2026. Pistrol, Adam & Schweiger (eds.)
Published by: ÖGG, Austrian Society for Geomechanics, Salzburg, Austria, ISBN 978-3-9503898-4-5
https://doi.org/10.53243/ICSMGE2026-133

Effects of the degree of saturation and density on the shear strength and stiffness of artificially frozen sand and gravel

Christos Vrettos, Elisabeth Seibel, Ronald Günther
Division of Soil Mechanics and Foundation Engineering, RPTU Kaiserslautern-Landau, Germany, vrettos@rptu.de

ABSTRACT: Artificial ground freezing is usually applied in water-saturated ground. Partial saturation significantly reduces the short- and long-term strength of frozen soil, particularly for loose sand and gravel. This may impair the stability of the frozen body; hence, a minimum value for the degree of saturation is often required. If this is not the case for the entire volume of the frozen body and controlled watering of the soil is not foreseen or feasible as a countermeasure, an estimate of the available strength of the frozen soil must be made. The paper reports on uniaxial and triaxial compression tests on unsaturated sand and sandy gravel to determine uniaxial compressive strength and creep behaviour, as well as shear strength parameters from triaxial compression tests. The strain-rate effects on strength and stiffness for the sandy gravel are investigated. The tests were performed in an apparatus with "on-the-device" cooling and temperature control instead of testing in a walk-in cold room. The experimental results confirm and complete the findings from the few previous studies. Empirical equations for the uniaxial compressive strength and modulus of elasticity in dependence on relative density, degree of saturation and strain rate are derived for use in practice.

KEYWORDS: ground freezing, unsaturated soil, laboratory testing.

1 INTRODUCTION

Artificial ground freezing was initially developed for constructing mining shafts and has been subject to ongoing development since its inception. Based on the experience of the last 40 years, it is now one of the standard methods used in civil engineering and tunnel construction as a temporary sealing or supporting structure. Still, planning and construction require special qualifications. The main areas of application are underpinning structures, underpassing buildings and railway tracks, securing short mining tunnels or the support of cross-passage excavations in tunnelling. A comprehensive overview of executed construction projects can be found in Böning et al. (1992), Kirsch & Richter (2009), Orth & Müller (2013), among other sources. The basics of the mechanical and thermal properties of the composite material "frozen ground" as well as details on the static and thermal design of the frozen body are described e.g. by Jessberger et al. (2002). Due to the tendency of frozen ground to creep, the long-term strength must be assessed in addition to the short-term strength, as it is often decisive for the design of the frozen body.

Artificial ground freezing is typically applied in water-saturated soils. In non-cohesive soils, such as sands and gravels, partial saturation can lead to a substantial decrease in the strength of the frozen body (Jessberger et al., 2002; Meissner & Vogt, 1991). Depending on the boundary conditions, degrees of saturation of 50 % to 70 % are specified as a lower limit to satisfy structural design requirements (Böning et al., 1992; Borkenstein et al., 1991). Controlled water enrichment (irrigation) of the unsaturated soil areas is an appropriate countermeasure (Böning et al., 1992; Jessberger et al., 2002). If this approach is not feasible or not desired for construction management reasons, reduced strength and stiffness must be accepted in the design of the frozen body. Information on the respective material parameters is scarce (Böning et al., 1992; Jessberger et al., 2002; Kuribayashi et al., 1985; Meissner & Vogt, 1991), and this was the primary motivation for conducting the present study.

In practice, uniaxial compression tests are the standard method for experimental investigation of frozen soils. This method is employed to assess the unconfined compressive strength, as well as the stiffness and the Poisson's ratio (Andersland & Ladanyi, 2004; Jessberger et al., 2002). These properties strongly depend on the temperature and the strain rate (Baker, 1979; Lee et al., 2016). Hence, a comprehensive testing program is necessary. Triaxial compression tests with variations of the cell pressure are much more complex (Da Re et al., 2003). True triaxial tests on cubic samples can also be performed to investigate specific loading paths that accurately reproduce in-situ conditions (Meissner & Kroh, 1994; Merz & Vrettos, 2015). In the aforementioned test devices, constant axial stress creep tests may also be conducted to assess the long-term strength, with failure being identified from the temporal variation of the creep strain (Jessberger et al., 2002; Ting et al., 1983). These tests can be conducted in one of two ways: either employing a suitable, complex device for cooling, insulating, and loading the specimen, or in a walk-in cold room with a controlled low-temperature environment.

To model the non-linear, time- and temperature-dependent material behaviour, elasto-viscoplastic constitutive models with varying degrees of complexity are utilised (Meissner & Vogt, 1991; Cudmani et al., 2022).

In the ensuing, laboratory tests on artificially frozen, partially saturated soil samples are presented with targeted variation of the degree of saturation and the relative density. Soils comprise sand and sandy gravel. As cooling was performed on the device, the experimental technique applied is described in addition to the results.

2 TEST EQUIPMENT AND TESTING PROCEDURES

2.1 *Devices*

All tests were carried out in a triaxial cell as shown in Figure 1. A Julabo FP55 SL ultra-low refrigerated circulator with a cooling capacity of +20 to -60 °C (using ethanol as the cooling liquid) was used for cooling. The apparatus is equipped with two cooling circuits: The first circuit utilises a cooling spiral system to cool the cell's interior, whereas the secondary circuit is responsible for cooling the base plate, see Figure 1. This is necessary because the heat generated by the hydraulic cylinder heats the base of the cell. Additionally, the apparatus allows freezing an initially unfrozen sample between the end platens in a single direction, from the bottom to the top. Depending on the ambient temperature, placing the specimen may lead to a minor temperature increase; the experiment starts only when the specimen and the device reach the target freezing temperature.

Temperatures as low as approximately -20 °C can be attained. The temperature measurement for regulating and controlling the cooling device is carried out at the same sampling rate as the recording of force and displacement.

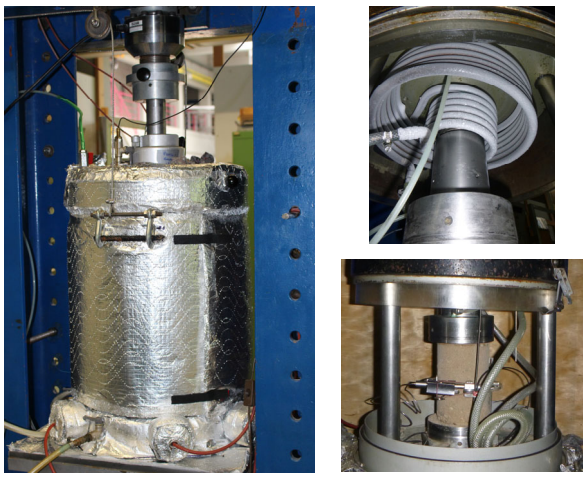

Figure 1. Triaxial device.

A Pt100 temperature sensor is placed directly on the latex rubber membrane surrounding the specimen at its mid-height. The triaxial cell temperature is also recorded visually via two temperature sensors at the level of the specimen top and the base platen level, at a distance of 6 cm from the specimen.

The device can perform both uniaxial and triaxial compression and creep tests. The maximum load is 200 kN for the axial force (axial stress 20 MPa for the standard specimen size) and 2 MPa for the lateral stress (cell pressure). In displacement-controlled tests, the testing machine typically achieves strain rates (percentage of specimen height per minute) ranging from 0.01 to 4.0 %/min. The cell is surrounded by a special insulating layer, as illustrated in Figure 1. The radial strain is measured at the specimen mid-height using a special measuring clamp, see Figure 1. The maximum measurable radial deformation is 10 mm. The vertical deformation is measured by a potentiometer with a measuring range between -17 mm and +17 mm (total of 34 mm). It is also possible to use an internal inductive displacement sensor with a measuring range up to 10 mm. This sensor records the displacement between the two end plates.

The cylindrical specimen has a standard diameter of 10 cm and a height of 15 cm. The end platens are lubricated as the height-to-diameter ratio is less than 2:1, as specified in the ISGF recommendations (Sayles et al., 1987). For this, a latex membrane is placed between the platen and the specimen. As this membrane hardens at sub-zero temperatures, it is first stored in oil before an additional layer of high-vacuum silicone grease is applied.

2.2 *Specimen preparation*

The specimens were frozen outside the device in a special cooling box under temperature control for 18 to 24 hours. To prevent residual freezing stresses within the specimen, freezing was performed in the axial direction along the height of the specimen. Before the installation in the triaxial cell, the specimen size is accurately measured. Afterwards, the specimen is covered with the latex membrane, and the clamp for measuring the radial displacement is attached.

2.3 *Distribution of water content within the specimen*

The problem of inhomogeneous water content distribution in partially saturated samples is well known. Older investigations in our laboratory on partially saturated, unfrozen sand (Becker, 2002) showed that the distribution varied over the specimen height after the end of the test. Compared to the initial state, a decrease was observed in the upper part and an increase in the lower part of the specimen. In that study, to determine the water content distribution, specimens were cut along the height, the material was carefully extracted, and the water content was determined at various points. Uneven distribution of water content inevitably prevails at low degrees of saturation.

In the present study, three distinct procedures were compared for sand to optimise the specimen preparation at low degrees of saturation. The water content was determined in the specimen's upper, middle, and lower thirds according to the procedure described above. The findings for an initial degree of saturation $S_r = 0.3$ and a dry density $\rho_d = 1.6$ g/cm^3 were as follows:

(i) With the conventional specimen preparation, water content distribution of 6.3/7.0/8.4 % was observed after two hours.

(ii) A second specimen, which was subjected to a 180° rotation immediately after preparation, exhibited a distribution of 7.2/7.2/7.6 % after two hours.

(iii) In the third variant, the specimen was rotated by 180° immediately after preparation and returned to its original position after two hours. After waiting another two hours, the water content amounted to 6.9/7.3/7.8 %.

At least for $S_r = 0.3$, the differences are of minor importance compared to the other inaccuracies in the testing procedure. Variant (ii) led to the highest degree of homogeneity. However, if the condition at the end of the test is also considered, (ii) can lead to a non-uniform distribution, as was observed in a fourth specimen with a water content distribution at the end of the test of 8.7/6.5/7.0 %.

When preparing sand specimens at $S_r = 0.45$, achieving a homogeneous water content distribution is much more difficult. This is because gravitational transport processes from the specimen's top towards the base increase with increasing water content. The exact evolution with time of such transport processes and the effects on the freezing process require further investigation. Degrees of saturation $S_r < 0.3$ are challenging, as a minimum amount of water is needed to prepare a frozen specimen.

For the test series with higher degrees of saturation, the soil was filled into a mould in three layers, placed in a water bath, and the water level was raised over several hours. As anticipated, the maximum achievable degree of saturation using that method was approximately 0.85. Homogeneity tests were not conducted for these high degrees of saturation.

3 MATERIAL TESTED

The soil material investigated consisted of several batches of uniformly graded sand (Sa) and well-graded sandy gravel (saGr) with 40 % to 50 % sand designated by saGr1, saGr3, and saGr4. For the identification and classification, we use EN ISO 14688-2:2018. Median grain diameter d_{50} and uniformity coefficient C_U were $d_{50} = 0.35...0.40$ mm and $C_U = 2.1...2.2$ for the sand and varied for the sandy gravel between $d_{50}/C_U = 1.6$ mm / 28.9 and 5.8 mm / 35.5. Figure 2 shows the average grain size distribution curve for the sand and the three curves for the sandy gravel.

For the tests on sandy gravel, grains larger than 32 mm were removed. In standard triaxial testing of non-uniform soil, the maximum grain size is usually limited to the 1/5 of the specimen diameter, i.e. 20 mm. As we are dealing here with the behaviour of frozen soil, this is not necessary, and maintaining the coarse grain size up to 32 mm yields a more representative composite material.

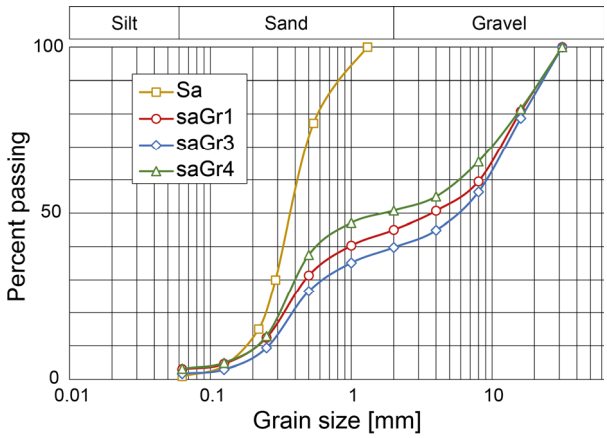

Figure 2. Grain size distribution of the material tested.

Minimum and maximum dry densities, $\rho_{d,min}$ and $\rho_{d,max}$, were determined to set the target relative density I_D in the tests. I_D is defined in terms of the void ratio according to EN ISO 14688-2:2018. Values for sand were $\rho_{d,min}/\rho_{d,max}$ = 1.42/1.82 g/cm³ and varied within a small range for the sandy gravels with $\rho_{d,min}/\rho_{d,max}$ = 1.89/2.13 g/cm³ to 1.87/2.07 g/cm³. Particle density for sand and sandy gravel was set equal to ρ_s = 2.65 g/cm³.

4 TESTING PROGRAMME AND RESULTS

4.1 *General*

The test series comprised uniaxial compression tests, uniaxial creep tests and a triaxial compression test.

The degree of saturation S_r and the relative density I_D were varied over a broad range.

For the sand: $0.3 < S_r < 0.9$; $0.2 < I_D < 0.51$

For the sandy gravels: $0.2 < S_r < 0.84$; $0.76 < I_D < 0.96$

Adjusting the relative density I_D to a pre-defined target value for the sandy gravels was difficult due to the small range between minimum and maximum density. Consequently, a slight change in density has a very strong influence on I_D. This is an inherent drawback related to the definition of I_D. Hence, for the sandy gravels, using the dry density value directly in specimen characterisation is more appropriate.

The temperature for all tests was set equal to T = -10°C.

4.2 *Uniaxial compression tests on sand and sandy gravel*

The uniaxial compression tests for assessing short-term strength were performed under strain-rate control. In practice, a strain rate of $\dot{\varepsilon}$ = 1%/min is typically selected in accordance with the ISGF recommendations (Sayles et al., 1987). Since lower strain rates yield lower strength, it was decided in the particular project to run most of the tests at $\dot{\varepsilon}$ = 0.1 %/min. To resolve project-specific issues, sandy gravels were also tested at lower and higher strain rates.

The tests performed and the results obtained are summarised in Table 1. The following notations are used: ρ_d is the initial dry density, σ_u is the unconfined compressive strength, $\varepsilon_{1,u}$ is the axial strain at failure. E_{50} is the Young's modulus defined as the secant modulus over the linear portion of the stress-strain curve up to 50 % of the ultimate stress σ_u. If this value lies outside the linear stress-strain range, E_{50} is determined up to the strain at which linear behaviour ends. The same procedure is used to define the starting point of the secant. To illustrate this evaluation procedure, the start and end points of the secant as well as the peak value are marked on two selected stress-strain curves in Figure 3.

Table 1. Uniaxial compression tests on sand and sandy gravel; $\dot{\varepsilon}$ = 0.1 %/min.

Test No.	Soil	ρ_d [g/cm³]	S_r [-]	I_D [-]	σ_u [MPa]	$\varepsilon_{1,u}$ [%]	E_{50} [MPa]
U1	Sa	1.52	0.298	0.22	0.86	2.16	62
U2	Sa	1.58	0.294	0.47	2.14	2.48	157
U3	Sa	1.59	0.298	0.49	2.48	2.42	165
U4	Sa	1.60	0.449	0.49	3.19	3.33	248
U5	Sa	1.59	0.596	0.49	4.95	3.05	518
U6	Sa	1.51	0.634	0.27	4.00	3.66	275
U7	Sa	1.60	0.837	0.51	7.20	5.05	1513
U8	Sa	1.55	0.874	0.39	8.15	4.65	1828
U9	saGr1	2.06	0.838	0.96	9.00	2.77	622
U10	saGr3	2.06	0.298	0.76	2.53	2.5	156
U11	saGr4	2.07	0.595	0.91	7.50	2.92	340
U12	saGr4	2.08	0.202	0.95	1.19	2.29	82
U13	saGr4	1.97	0.300	0.52	3.21	1.94	230

The results demonstrate a strong reduction in compressive strength with decreasing degree of saturation. For example, from the tests U2, U5, and U7, one may see the following trend for $I_D \approx 0.5$: The uniaxial strength amounts to σ_u = 7.2 MPa for S_r = 0.84 and drops down to σ_u = 4.95 MPa for S_r = 0.6, and further down to σ_u = 2.14 MPa for S_r = 0.29.

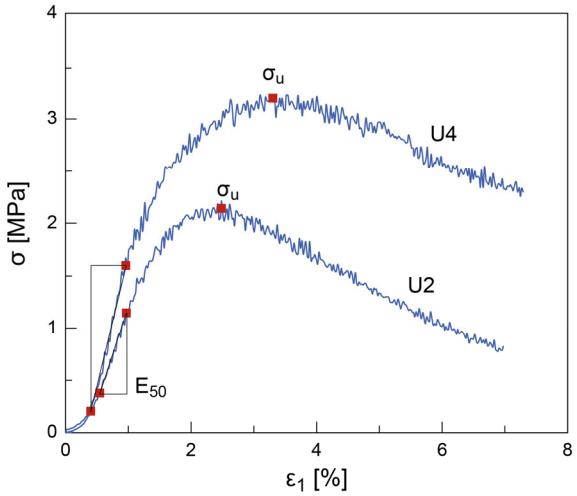

Figure 3. Selected stress-strain curves from two uniaxial compression tests on sand; $\dot{\varepsilon}$ = 0.1 %/min.

The maximum compressive strength in the test series on sand amounted to σ_u = 8.15 MPa and was obtained for S_r = 0.87 and medium dense condition I_D = 0.39 (test U8), while the lowest value, σ_u = 0.86 MPa, was measured for S_r = 0.30 and loose condition I_D = 0.22 (U1). The difference is significant (a factor of almost 10).

Figure 4 displays the values of σ_u for sand as a function of the degree of saturation S_r for the two relative density ranges. The data for $0.3 \le S_r \le 0.9$ can be approximated very well by linear functions:

Sand I_D = 0.22...0.27 $\sigma_u = 9.4 \cdot S_r - 2.0$ (1)

Sand I_D = 0.47...0.51 $\sigma_u = 9.4 \cdot S_r - 0.63$ (2)

with σ_u given in [MPa].

Figure 4 also includes the results for the sandy gravels at $\dot{\varepsilon}$ = 0.1 %/min. The data also exhibit a linear dependence on S_r with the same slope as for the sand:

sandy Gravel I_D = 0.76...0.96 $\sigma_u = 9.4 \cdot S_r + 0.87$ (3)

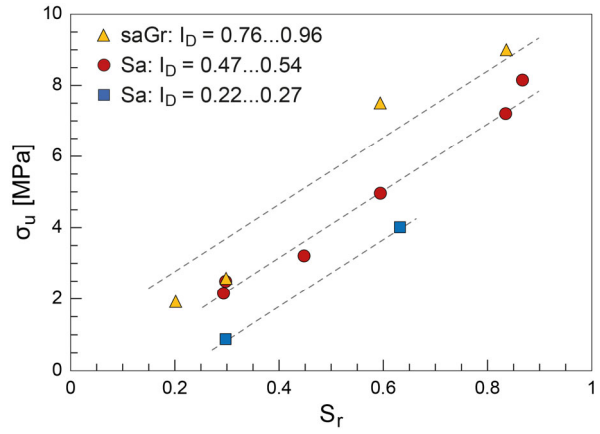

Figure 4. Uniaxial compression strength σ_u dependent on the degree of saturation S_r for sand and sandy gravel; $\dot{\varepsilon} = 0.1$ %/min. The dashed lines are for the approximation by Equations (1), (2), and (3), respectively.

The findings from Böning et al. (1992) for medium relative density and $\dot{\varepsilon} = 1$ %/min (tests conducted in a cold room) are used for verification, although in that study no differentiation between sands and gravels was made in the report. The results confirm the linear decrease in strength with decreasing degree of saturation, with a good agreement between the individual data. A further comparison is made with the test results on sand ($d_{50} = 0.4$ mm, $C_U = 2.53$) reported by Kuribayashi et al. (1985), some of which are also presented in Andersland & Ladanyi (2004). In that study, cooling was also carried out on the device as described above. The back-calculated density is $\rho_d = 1.4$ g/cm³, but information on $\dot{\varepsilon}$ is missing, and the approximation of the results derived by Andersland & Ladanyi (2004) is not accurate. At $T = -10$ °C and $S_r = 0.54$, the data in Kuribayashi et al. (1985) yield $\sigma_u \approx 4.8$ MPa. In good agreement, Equation (2) predicts $\sigma_u = 4.45$ MPa.

Regarding the axial strain at peak $\varepsilon_{1,u}$, sand specimens with a low degree of saturation, $S_r \approx 0.3$, exhibit the smallest values, see tests U2, U6, and U7. No clear trend is observed for the sandy gravels, with the values varying within a narrow range.

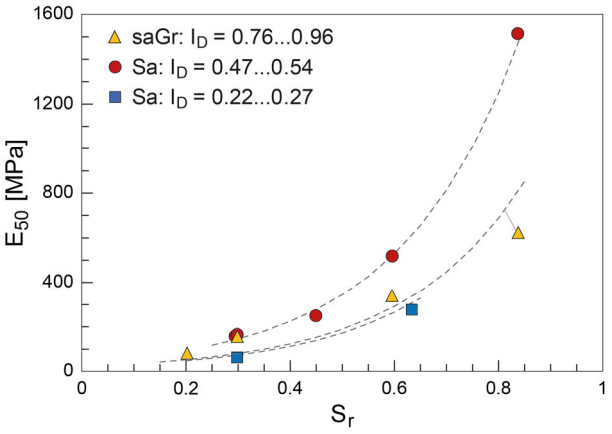

Figure 5. Variation of modulus E_{50} with the degree of saturation S_r in the uniaxial compression tests on sand and sandy gravel; $\dot{\varepsilon} = 0.1$ %/min. The dashed lines are for the approximation by Equations (4), (5), and (6), respectively.

Next, we compare the results for the secant modulus E_{50}. Both sand and sandy gravel exhibit a decrease with decreasing degree of saturation, as illustrated in Figure 5. The data for $\dot{\varepsilon} = 0.1$ %/min can be approximated by an exponential function, and adjusting merely the proportionality factor yields:

Sand $I_D = 0.22...0.27$ $E_{50} = 20 \cdot \exp(4.3 \cdot S_r)$ (4)

Sand $I_D = 0.47...0.51$ $E_{50} = 40 \cdot \exp(4.3 \cdot S_r)$ (5)

sandy Gravel $I_D = 0.76…0.96$ $E_{50} = 22 \cdot \exp(4.3 \cdot S_r)$ (6)

with E_{50} in [MPa]

4.3 *Effects of strain rate*

As mentioned above, sandy gravel was tested under various strain rates ranging from 0.01 %/min to 4.0 %/min. Figure 6 displays, in a semi-logarithmic plot, the results at different combinations of S_r and I_D. We refrain herein from tabulating the individual data for the sake of conciseness. It can be clearly seen that increasing the loading rate increases the compressive strength. To derive a simple, even rough approximation, we divide the data by the respective value at $\dot{\varepsilon} = 0.1$ %/min as measured in the tests (Table 1), and approximate the normalised data by a logarithmic function, yielding:

$$\sigma_u(\dot{\varepsilon}) = \sigma_u(\dot{\varepsilon}=0.1) \cdot [0.08 \cdot \ln(\dot{\varepsilon}) + 1.2] \quad (7)$$

with $\dot{\varepsilon}$ in %/min. This function is plotted in Figure 6 to visualise the quality of the approximation.

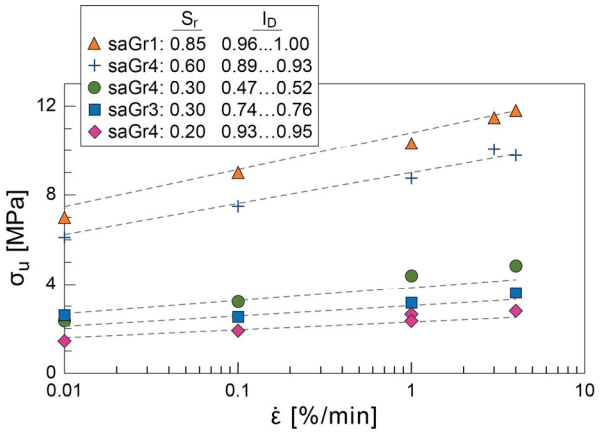

Figure 6. Uniaxial compression strength σ_u for the sandy gravels dependent on the strain rate $\dot{\varepsilon}$. The dashed lines are for the approximation by Equation (7).

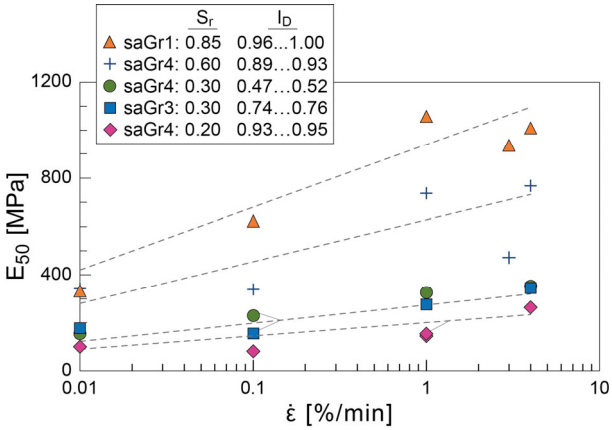

Figure 7. Secant modulus E_{50} for the sandy gravels, dependent on the strain rate $\dot{\varepsilon}$. The dashed lines are for the approximation by Equation (8).

The test results for the sandy gravel may also be used to derive an expression for the variation of the secant modulus E_{50} with strain rate. Just like for the compressive strength, we first normalise the results to those for $\dot{\varepsilon} = 0.1$ %/min, Equation (6), and then assume a logarithmic variation with the strain rate. Contrary to the compressive strength, we need to capture the influence of S_r by a separate function to reach a good

approximation. By visual inspection, we derive the following expressions for the sandy gravel (E_{50} in MPa and $\dot{\varepsilon}$ in %/min):

$$E_{50} = E_{50}(\dot{\varepsilon}=0.1) \cdot [4.7 \cdot (1 - 0.9 \cdot S_r) \cdot (1 + 0.12 \cdot \ln(\dot{\varepsilon}))] \quad (8)$$

The experimental data and the approximations are compared in Figure 7. One may see that the scatter in the data is much larger for the secant modulus E_{50} than for the compressive strength σ_u.

4.4 *Uniaxial creep tests on sand*

In the tests on sand, the creep stress σ_{cr} was set equal to a percentage of the previously determined compressive strength, or it was specified directly based on design criteria. Loading up to the target creep stress level was carried out in small load steps. An inflexion point in the creep strain vs. time curve defines the creep failure (Ting et al., 1983). The associated time to minimum strain rate, t_m, is determined from the creep rate vs. time curve, $\dot{\varepsilon}_1(t)$. The associated axial strain is denoted by $\varepsilon_{1,m}$. An overview of all test setups and results is given in Table 2.

The test series primarily focused on $S_r = 0.30$ and $I_D = 0.50$. The respective unconfined compressive strength σ_u, calculated from the average of tests U2 and U3, equals 2.31 MPa. For C5, with $S_r = 0.5$ and $I_D = 0.50$, σ_u was taken from U4. Thus, the creep stress in the tests varied between 29% and 56% of σ_u.

Table 2. Uniaxial creep tests on sand.

Test No.	Soil	ρ_d [g/cm³]	S_r [-]	I_D [-]	σ_{cr} [MPa]	σ_{cr}/σ_u [-]	t_m [h]	$\varepsilon_{1,m}$ [%]
C1	Sa	1.58	0.295	0.47	1.29	0.56	1.9	3.22
C2	Sa	1.59	0.298	0.49	0.67	0.29	19.1	1.73
C3	Sa	1.59	0.297	0.49	1.30	0.56	9.7	2.12
C4	Sa	1.59	0.298	0.49	0.98	0.42	4.1	3.09
C5	Sa	1.61	0.455	0.52	1.06	0.33	6.2	2.16

Figure 8 shows a typical creep curve. The creep rate is determined by numerically differentiating the creep strain vs. time curve. Although the creep curve appears uniform in the plots, numerical differentiation of the raw data yields an irregular curve. For better visualisation, the creep strain curves are smoothed before differentiation, as are the calculated creep rate curves. Data pairs (t_m; ε_{1m}) are marked in the plots of Figure 8.

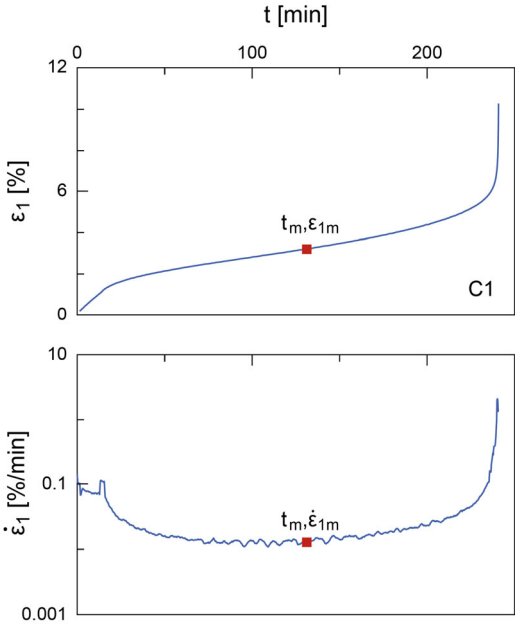

Figure 8. Creep curves form test C1 on sand with an indication of time to minimum strain rate, t_m.

The results indicate that the lowest creep stress results in a significantly longer time to failure, as observed, for example, in test C2. The comparison between C1 and C3 shows that the results vary considerably under the same conditions (density, degree of saturation, creep stress). However, the t_m-values are significantly shorter than those of fully saturated specimens. In practical applications, where stability of the frozen body over several days is required, differences in the range of hours are of minor importance. Due to the limited data available for unsaturated soil, it is difficult to make reliable predictions of the time to creep failure.

The dramatic decrease in the sustainable creep stress at low saturation levels is demonstrated by the curves in Figure 9. The relationship between creep stress, σ_{cr}, and time to creep failure, t_m, is presented in a semi-logarithmic plot. In addition to the test results, the limiting curves for fully saturated sands according to Orth (1988), which were derived from creep tests at -20 °C and -2 °C, are shown for comparison. If the σ_{cr}-t_m relationship given in that reference is applied, the test results at $S_r = 0.3$ correspond to a freezing temperature of approximately -0.4 °C at $S_r = 1$.

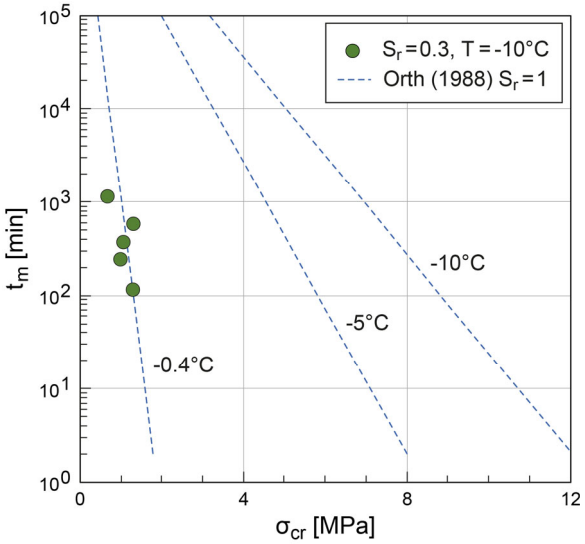

Figure 9. Variation of time to minimum strain rate, t_m, with creep stress for sand. Data points represent the test results for $S_r = 0.3$ at $T = -10$°C, the dashed lines the relationship for $S_r = 1$ at different temperatures from Orth (1988).

4.5 *Triaxial compression tests on sand*

Triaxial compression tests were conducted on frozen sand to determine the shear strength parameters for the subsequent constitutive modelling of the frozen body at a low relative density $I_D = 0.2$ and a low degree of saturation $S_r = 0.3$. This combination was selected to simulate the most unfavourable condition regarding bearing capacity. The testing technique corresponds to the procedure for the uniaxial compression tests with the additional application of a cell pressure σ_3. The strain rate was set equal to 0.1 %/min. The peak axial stress at failure σ_{1p} and the corresponding axial strain ε_1 were obtained from the tests. The results are summarised in Table 3.

Table 3. Triaxial compression tests on sand; $\dot{\varepsilon} = 0.1$ %/min.

Test No.	Soil	ρ_d [g/cm³]	S_r [-]	I_D [-]	σ_3 [MPa]	σ_{1p} [MPa]	φ_p [°]	c [MPa]
T1	Sa	1.524	0.306	0.18	0.15	1.40	30.8	0.27
		1.534	0.311	0.26	0.30	1.70		
		1.522	0.305	0.20	0.45	2.27		

For the evaluation, pairs of values (σ_{1p}; σ_3) at the peak state are approximated by a linear relationship, $\sigma_{1p} = A \cdot \sigma_3 + B$, adopting

a Mohr-Coulomb failure criterion. In this relationship, $A = (1+\sin\varphi_p) / (1-\sin\varphi_p)$ and $B = 2 \cdot c \cdot \sqrt{A}$. A and B are obtained by regression analysis. The peak friction angle φ_p and the cohesion c are then calculated from A and B. From the test, we obtain: $\varphi_p = 30.8°$ and $c = 0.27$ MPa. The photograph in Figure 10 shows that at such a low degree of saturation, frozen sand exhibits a shear behaviour similar to unfrozen soil.

Figure 10. Sand specimen at the end of the triaxial test T1 at $\sigma_3 = 0.3$ MPa; $\dot{\varepsilon} = 0.1$ %/min.

5 CONCLUSIONS

A reduction in the degree of saturation leads to a significant decrease in short- and long-term strength both in sand and in sand-gravel mixtures. For instance, at medium relative density, the unconfined compressive strength at 40 % saturation is approximately 50 % of the value at 80 % saturation. This effect is particularly evident in the context of creep behaviour, as indicated by a substantial reduction in the time to reach an inflexion point in the creep curve (time to failure) and the associated strain. A decrease in relative density has been shown to result in a reduction in strength. The experimental findings indicate that frozen soil exhibits not only cohesion but also substantial internal frictional resistance. All experimental findings refer to a temperature of -10 °C, and further investigations are necessary to capture the effects of temperature.

Given the complex specimen preparation process, which includes variable bulk density and saturation, as well as the inherent inhomogeneity of the prepared sand and sandy gravel specimens, and the complex testing technique, the variation in the results is small. The “on-the-device” testing technique facilitates the execution of triaxial tests, yielding reproducible results that are in good agreement with those reported in other studies.

The derived approximate expressions may be employed to assess the effects of relative density, degree of saturation, and strain rate in practice.

6 REFERENCES

Andersland, O.B. and Ladanyi, B., 2004. *Frozen Ground Engineering.* 2nd Edition. Hoboken, N.J.: John Wiley & Sons.

Baker, T. H. W., 1979. Strain rate effect on the compressive strength of frozen sand. *Engineering Geology*, 13, 223-231.

Becker, A., 2002. *Stoffmodell und numerisches Modell für zyklisch beanspruchte, teilgesättigte Sande.* Veröffentlichungen des Fachgebiets Bodenmechanik und Grundbau der Universität Kaiserslautern.

Böning, M., Jordan, P., Seidel, H.-W. and Uhlendorf, W., 1992. Baugrundvereisung beim Teilbaulos 3.4 H der U-Bahn Düsseldorf. *Bautechnik*, 69(12), 693-705.

Borkenstein, D., Jordan, P. and Schäfers, P., 1991. Construction of a shallow tunnel under protection of a frozen soil structure, Fahrlachtunnel at Mannheim, Germany. In: Yu, X., Wang, C., eds. *Ground Freezing 91 - Proceedings of the 6th International Symposium on Ground Freezing*. Beijing. Rotterdam: A.A. Balkema, Vol. 2, 481-487.

Cudmani, R., Yan, W. and Schindler, U., 2022. A constitutive model for the simulation of temperature-, stress- and rate-dependent behaviour of frozen granular soils. *Géotechnique*, 73(12), 1043-1055.

Da Re, G., Germaine, J. and Ladd, C.C., 2003. Triaxial testing of frozen sand: Equipment and example results. *Journal of Cold Regions Engineering*, 17(3), 90-118.

Jessberger, H. L., Jagow-Klaff, R. and Braun, B., 2002. Ground freezing. In: Smoltzcyk, U., ed. *Geotechnical Engineering Handbook, Vol. 2: Procedures.* Berlin: Ernst & Sohn, 117-167.

Kirsch, F. and Richter, T., 2009. Ground freezing for tunnelling under historical structures. In: *Proceedings of the 17th International Conference on Soil Mechanics and Geotechnical Engineering*. Alexandria, 2487-2490.

Kuribayashi, E., Kawamura, M. and Yui, Y., 1985. Stress-strain characteristics of an artificially frozen sand in uniaxially compressive tests. In: Kinosita, S., Fukuda, M., eds. *Ground Freezing 85 - Proceedings of the 4th International Symposium on Ground Freezing*. Sapporo, Sapporo: Hokkaido University Press, 177-182.

Lee, J., Kim, Y.S., Chae, D. and Cho, W., 2016. Loading rate effects on strength and stiffness of frozen sands. *KSCE Journal of Civil Engineering*, 20(1), 208-215.

Meissner, H. and Kroh, H., 1994. Plastic and viscous potential of frozen sand. In: Fremond, M., ed. *Ground Freezing 94 - Proceedings of the 7th International Symposium on Ground Freezing*. Nancy, France. Rotterdam: A.A. Balkema, 181-187.

Meissner, H. and Vogt, J., 1991. Tunnel construction in the protection of a frost cell in partially saturated soil. In: Yu, X., Wang, C., eds. *Ground Freezing 91 - Proceedings of the 6th International Symposium on Ground Freezing*. Beijing. Rotterdam: A.A. Balkema, 337-344.

Merz, K. and Vrettos, C., 2015. Materialverhalten von gefrorenem Sand aus Triaxialversuchen an kubischen Proben. In: Schanz, T., Hettler, A., eds. *Aktuelle Forschung in der Bodenmechanik 2015.* Berlin, Heidelberg: Springer Vieweg, 101-117.

Orth, W. and Müller, B., 2013. Temporary watertight connection of excavations to existing buildings and temporary waterproofing of structures by ground freezing. *Geomechanics and Tunnelling,* 6(3), 246-260.

Orth, W., 1988. A creep formula for practical application based on crystal mechanics. In: Jones, R. H., Holden, J. T., eds. *Ground Freezing 88 - Proceedings of the 5th International Symposium on Ground Freezing*, Nottingham. Rotterdam: A. A. Balkema, 205-211.

Sayles, F. H., Baker, T. H. W., Gallavres, F., Jessberger, H. L., Kinosita, S., Sadovskiy, A. V., Sego, D., Vyalov, S. S., 1987. Classification and laboratory testing of artificially frozen ground. *Journal of Cold Regions Engineering*, 1(1), 22-48.

Ting, J.M., Martin, R.T. and Ladd, C.C., 1983. Mechanisms of strength for frozen sand. *Journal of Geotechnical Engineering*, 109(10), 1286-1302.